Influence of material heterogeneity on the mechanical response of articulated cartilages in a knee joint

Vaishakh Raju[a] and Poornesh K Koorata[a,*]

[a]*Applied Solid Mechanics Laboratory, Department of Mechanical Engineering, National Institute of Technology Karnataka, Surathkal 575025, India;*

*Corresponding Author

Poornesh K Koorata
Applied Solid Mechanics Laboratory, Mechanical Engineering Department,
National Institute of Technology Karnataka, Surathkal 575025, India.
Email: kpkoorata@nitk.edu.in
Tel.: +91-824-247-3650
Fax: +91-824-247-4003

Abstract

Structurally, the articular cartilages are heterogeneous owing to nonuniform distribution and orientation of its constituents. The oversimplification of this soft tissue as a homogeneous material is generally considered in the simulation domain to estimate contact pressure along with other physical responses. Hence, there is a need for investigating knee cartilages for their actual response to external stimuli. In this article, impact of material and geometrical heterogeneity of the cartilage is resolved using well known material models. The findings are compared with conventional homogeneous models. The results indicate vital differences in contact pressure distribution and tissue deformation. Further, this study paves way for standardising material models to extract maximum information possible for investigating knee mechanics with variable geometry and case specific parameters.

Keywords: Articular cartilage; Contact Pressure; Finite element analysis; Knee joint; Material heterogeneity; Superficial layer;

1. Introduction

The knee is a complicated joint that includes tibiofemoral and patella-femoral articulations[1,2]. Mechanically, articular cartilage functioning similar to frictionless bearing between the surfaces[3]. The knowledge of contact pressure and stress fields is essential in predicting the onset of functional damage of these tissues[4–6]. The computational model for whole-knee biomechanics is a useful clinical tool for determining the onset and progression of disease and injury. The critical challenge in simulating soft tissues like articular cartilage is the complexity of structure, compounded by the heterogeneous distribution of collagen fibers throughout its cross-section[7,8]. A dense extracellular matrix (ECM) with a random distribution of

chondrocyte cells constitutes the cartilage structure. ECM is primarily composed of collagen fibers, proteoglycan, and water fraction[9]. These components jointly help maintain ECM water, critical in keeping properties like sudden impact strength and high compressive strength[10]. A cross-section of articular cartilage reveals the direction of collagen fibers into three zones: fibers oriented parallel to articulating surface in the superficial zone (SZ), randomly oriented in transitional zone (TZ) and oriented perpendicular to subchondral bone in the deep zone (DZ) [11,12]. The zonal thickness of SZ, TZ, and DZ is about 12%, 32%, and 56% of cartilage's total thickness, respectively [13].

The most common material models for simulating the mechanical behavior of cartilage are isotropic elastic (IE), isotropic poroelastic (IPE), transversely isotropic poroelastic/ transversely isotropic elastic (TIPE/TIE), and fibril-reinforced poroviscoelastic/poroelastic (FRPVE/FRPE) [10,14,23,15–22]. The isotropic elastic model predicts the instantaneous cartilage response faster compared with its alternative models [24–27]. Essentially these models give a qualitative understanding of the response. Nevertheless, in reality, articular cartilages comprise a porous matrix saturated with water (68% - 88% of cartilage weight). The response of cartilage tissue is influenced by fluid pressure, according to studies [28,29]. Hence the biphasic characteristics of cartilage are generally studied with IPE models. In IPE models, the fluid flow in cartilage is modelled with Darcy's law related to permeability(k) [30].

Apart from biphasic characteristics, the articular cartilage constitutes a non-fibril matrix and collagen fibril network. FRPE model may suit well to simulate the response of such structure[31]. The material orientation is assigned such that it mimics contribution of collagen fibril orientation (arcade-like structure). However, this model is computationally not cost effective, lacks their relevance in clinical applications. TIE

models are also widely used in modelling articular cartilage[32–34]. From recent studies, the TIE model can predict intact articular cartilage uniaxial compression responses with higher accuracy [35]. The highly heterogeneous nature of superficial zone can simulate well with such models[36,37] the most influential compartment on articular cartilage to mechanical response [38].

Although many studies were conducted on the articular cartilage behavior with multiple constitutive models [39–44], the mechanical response of heterogeneous cartilage at maximum loading position in a gait is not adequately compared. Therefore, our primary objective is to address this issue by considering graded cartilage material with multiple heterogeneous constitutive models. The scope of the paper extends further to identify the critical differences among material models in predicting contact pressure and stress distributions. Even though the cartilage structure is complex and comprises dense collagen fibre networks and extracellular matrixes, the hypothesis addressed for the current study assumes cartilage as elastic models. The present study focused on the tibio-femoral articulation, ignoring the effects of muscle, tendon, and patella forces on cartilage response prediction at full extension position in a gait cycle.

2. Materials and Methods

2.1 Geometry and Finite Element model

An existing knee joint geometry (open knee) developed at Computational Bio modeling Core and Department of Biomedical Engineering, Cleveland Clinic from a female corpse (70 years & 77 kg) is used for the current study [45,46]. An expanded view of knee geometry (Figure 1(a)) and the 3D knee substructure is imported into Abaqus CAE for analysis. The model contains four ligaments anterior and posterior cruciate ligaments (ACL and PCL) and medial and lateral collateral ligaments (MCL and LCL), two

cartilages (femur and tibia cartilage), two meniscus (lateral and medial meniscus) and two bones (femur and tibia).

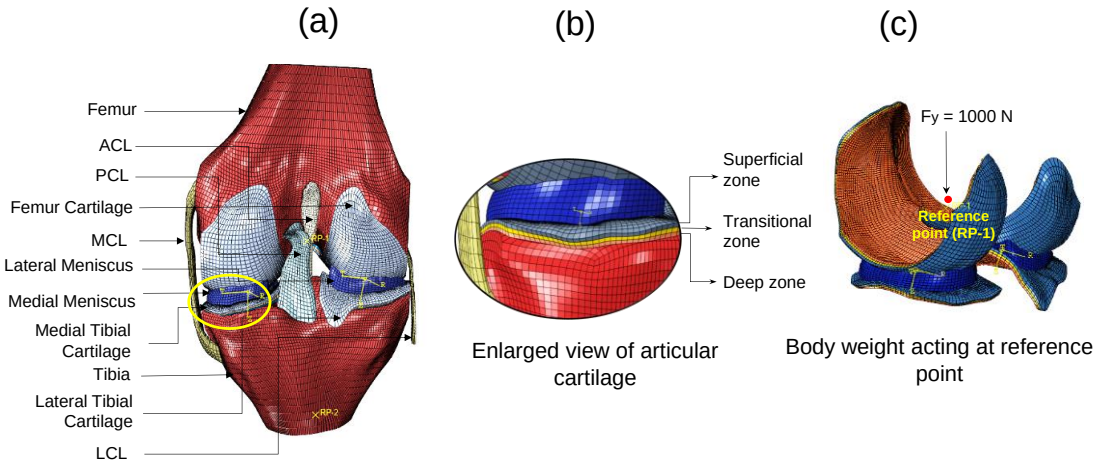

Fig 1. (a) The posterior view of 3D finite element knee joint model (b) enlarged view of tibial cartilage with three layers in different colours representing inhomogeneity; (c) Bodyweight acting on knee joint simulated by applying 1000N force in vertical direction acting downwards at the reference point which is constrained with femur cartilage and meniscus.

The coordinate system of the geometry is synchronized with the Abaqus, such that the x-axis is anterior-posterior, where the anterior or posterior force component can apply. Similarly, the y-axis is the proximal-distal where the vertical ground reaction force can use, and the z-axis is the medial-lateral direction where medial or lateral joint force components can apply. The ground reaction force becomes the body weight (BW) when the body is in a full extension position during the stance phase of a gait cycle. The valgus or varus rotation is about the x-axis, internal or external rotation is about the y-axis, and the flexion or extension rotation is about the z-axis.

In this article, the heterogeneity of the cartilage is defined in terms of material and geometrical heterogeneities. The material heterogeneity is the inhomogeneous distribution of material constituents (such as fiber density and orientation) and it is modeled using the corresponding constitutive models. The geometrical heterogeneity is

the inhomogeneity in terms of cartilage structure (such as superficial, transverse/middle, and deep zones) as shown in Figure 1(b). It may be noted here is that native architecture of cartilage may have these individual layers with different thicknesses depending on the collagen fiber structural inhomogeneity. The current study, however, assumes mesh size of each zone is to be same for numerical convergence purpose. These soft tissues are discretized into 56433 hexahedral elements with an element size of 0.5 mm each. The cartilage, meniscus, and ligaments are meshed with hexahedral brick elements (element type: C3D8) and the femur and tibia are meshed with shell elements (element type: S4) as per Abaqus/Standard user's manual [47]. The use of an 8-node element in contact modelling has the potential to improve contact response and numerical convergence than higher node elements.

2.2 Interface, constraints, loading and boundary conditions

The interaction between the cartilages at the articulating surface is assigned as frictionless contact. A rigid body tie constraint ties the ligaments and cartilage with bone's nodes at the bone insertion points to retain their position. Another rigid body constraint connects the tibia and femur to corresponding reference points (RP-1 and RP-2), such that the tibia and femur act as rigid body. The RP-1 is at the centre position of lateral and medial femoral epicondyles for the femur. The femur can rotate about RP-1, and the meniscus is constrained such that its position is maintained between two cartilages.

All rotational and linear motions (6DOF) of tibia is constrained and the femur is set free to move in all five degrees of freedom but restricted in knee flexion. Since this study focus on the maximum extension position of gait cycle, when flexion angle is zero. Thus RP-1 is subjected to a load of 1000N (compressive) as shown in Figure 1(c)

2.3 *Material Models*

The influence of homogeneous and heterogeneous (both material and geometrical case) cartilage surface texture is compared for mechanical response using well-known material models. These are IE, IPE, and TIE models. Note that the basic models such as IE and IPE assumes collagen fibers is homogenized with rest of the cartilage constituents. The TIE model is extended version of these basic models where collagen contribution is assumed as reinforcements. The material constants of these models (the constitutive relation of all these models are given supplementary information S1) are provided in Table 1.

Table 1

The material parameters used for modeling homogeneous and heterogeneous articular cartilage.

Material models	**Homogeneous** ***(non-gradient)***	**Heterogeneous** ***(gradient)***	**Source**
IE	$E = 15$ MPa $\nu = 0.475$	$E_s = 15$ MPa $E_t = 10$ MPa $E_d = 5$ MPa $\nu = 0.475$	[27]*
IPE	$E = 15$ MPa $\nu = 0.475$ $S_l = 1$ $e = 4$ $k = 0.001\, mm^4/Ns$	$E_s = 15$ MPa $E_t = 10$ MPa $E_d = 5$ MPa $\nu = 0.475$ $S_l = 1, e = 4$ $k = 0.001\, mm^4/Ns$	[27,48]*
TIE	$E_p = 5.8\, MPa$ $E_t = 0.46\, MPa$ $\nu_p = 0.87\,(-)$**	$E_{ps} = 5.8\, MPa$ $E_{ts} = 0.46\, MPa$ $\nu_{ps} = 0.87\,(-)$ $\nu_{ts} = 0.03(-)$	[29,49,50]*

	$\nu_t = 0.03(-)$	$G_{ts} = 2.5\ MPa$
	$G_t = 2.5\ MPa$	
	$E_{pt} = 4\ MPa$	
	$E_{tt} = 0.46\ MPa$	
	$\nu_{pt} = 0.87\ (-)$	
	$\nu_{tt} = 0.05(-)$	
	$G_{tt} = 2\ MPa$	
	$E_{pd} = 2\ MPa$	
	$E_{td} = 0.46\ MPa$	
	$\nu_{pd} = 0.87\ (-)$	
	$\nu_{td} = 0.2\ (-)$	
	$G_{td} = 1\ MPa$	

158 Notes: E = Elastic modulus, ν = Poisson's ratio, E_s, E_t, E_d = Elastic moduli of the superficial,
159 transitional and deep layer, E_{ps}, E_{pt}, E_{pd} and E_{ts}, E_{tt}, E_{td} are in-plane and out of plane
160 Young's moduli for the three layers, similarly $\nu_{ps}, \nu_{pt}, \nu_{pd}$ and ν_{ts}, ν_{tt}, ν_{td} are in-plane and out
161 of plane Poisson's ratio for the three layers. G_{ts}, G_{tt}, G_{td} are out of plane shear modulus for all
162 layers respectively, S_l = specific weight of wetting liquid, k = permeability and e = void ratio.
163 *Source for the homogeneous (non-gradient) model.
164 **Poisson's ratio in the in-plane direction has been chosen from article [29], but the value is
165 altered to match the material's consistency in Abaqus.

166 The rest of the joint parts are modelled as per Table 2. Even though the bone
167 (femur and tibia) consists of the cortical and cancellous parts, we approximated it as a
168 uniform rigid body. Similar to articular cartilage, the meniscus also has complicated
169 architecture, including a network of collagen fibers. To reduce the complexity in
170 modelling, we modelled the meniscus (lateral and medial) with TIE material [51]. The

ligaments are modeled with Neo-Hookean isotropic hyperelastic material (nearly incompressible) model.

Table 2

The material parameters for the components of the knee joint other than cartilage

Parts	Components	C_1 (MPa)	D_1 $(MPa)^{-1}$	Source
Ligaments isotropic hyperelastic (Neo-Hookean)	ACL	1.95	0.00683	[52,53]
	PCL	3.25	0.0041	
	MCL	1.44	0.00126	
	LCL	1.44	0.00126	
Meniscus (TIE)	$E_p = 120\ MPa, E_t = 20\ MPa$ $\nu_p = 0.2\ (-), \nu_t = 0.3(-)$ $G_p = 8.33\ MPa, G_t = 57.7\ MPa$			[53]

Notes: C_1 and D_1 are Neo-Hookean material constants, $E_p$and E_t are in-plane and transverse plane elastic modulus, ν_p and ν_t are in-plane and transverse plane Poisson's ratio, $G_p$and G_t are in-pane and transverse plane shear modulus.

3. Results

The contact pressure distribution in the tibial cartilage surface from the meniscus impact are compared for homogeneous and heterogeneous cartilage cases are given in Figure 2. Though no significant difference is observable in Figure 2(a), the homogeneous model provides higher contact pressure distribution compared to heterogeneous case. Among all the constitutive models compared, TIE and IPE models shows a clear impression of contact pressure on the cartilage surface.

Also the equivalent stress has an essential role in predicting knee pathologies. Figure 3(a) depicts the stresses distribution on the tibial surface. Compared with the IE and TIE model, the IPE model showed maximum equivalent stress generated in the femur cartilage. This indicates the biphasic tissue model supports more load than the simple model during the load transfer mechanism. Also it is observed here that the IE and IPE geometrical heterogeneous models provide less uniformity in stress distribution with respect to the TIE model. Figure 3(b) shows the femoral stress distribution and it follows similar pattern for all models, where the TIE model gives a clear understanding of the stress impression with no stress concentration. The maximum stress generated on the TIE model are 2.559 MPa and 2.792 MPa for the tibial cartilage, 2.045 MPa and 2.231 MPa for the femoral cartilage for the material heterogeneous and homogeneous cases, respectively.

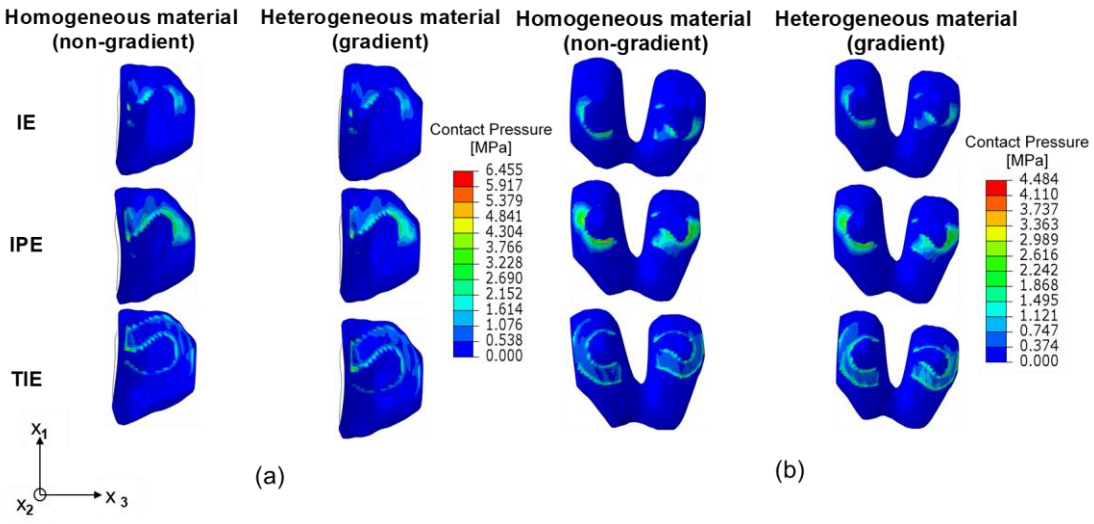

Fig 2. Distribution of contact pressure on (a) the tibial lateral surface; (b) the femoral surface

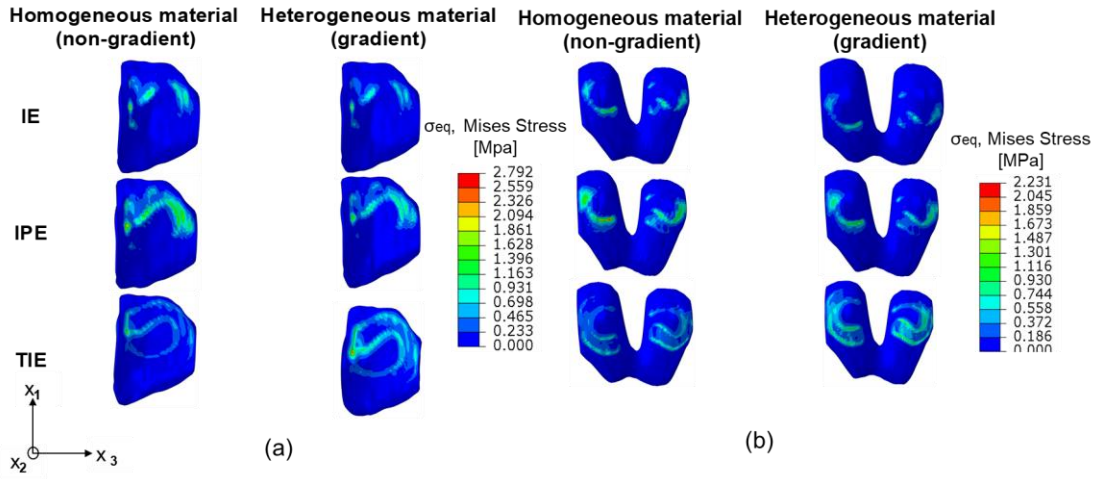

Fig 3. The contours for equivalent stress generation on (a) the tibial lateral surface; (b) the femoral surface

Directional stress may give better insights into the knee mechanics. Figure 4(a) and 4(b) clearly distinguish the directional stress impression in tibial and femoral surface. Figure 4(a) shows a uniform stress distribution in heterogeneous (both material and geometrical) case for all models compared to homogeneous model. In TIE model the tibial cartilage has a lower stress than the femur cartilage -2.2 MPa and -1.4 MPa respectively. Also the compression stress in the homogeneous situation is relatively high for the TIE model. This could be owing to the high rigidity provided by the cartilage's surface.

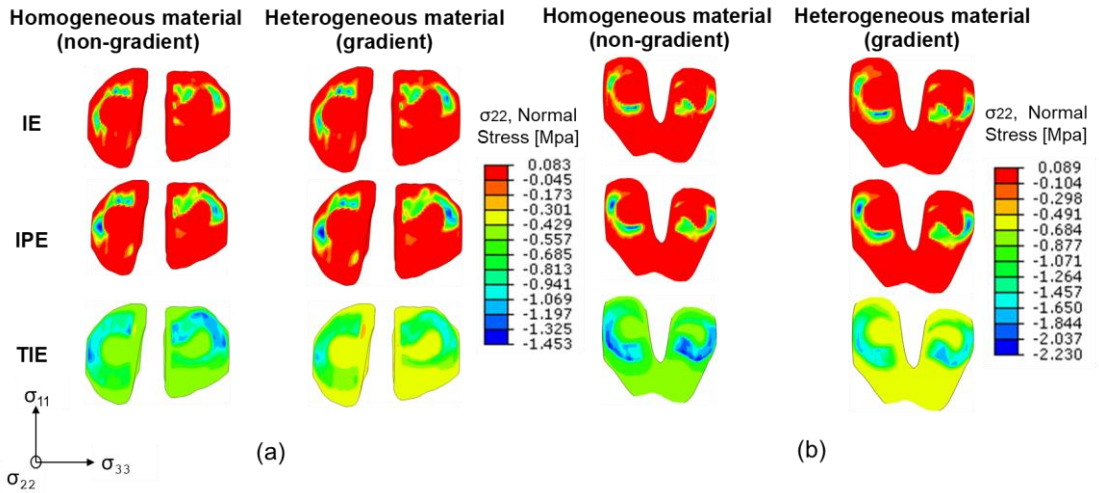

Fig 4. The normal stress distribution on (a) the tibial surface; (b) the femoral surface

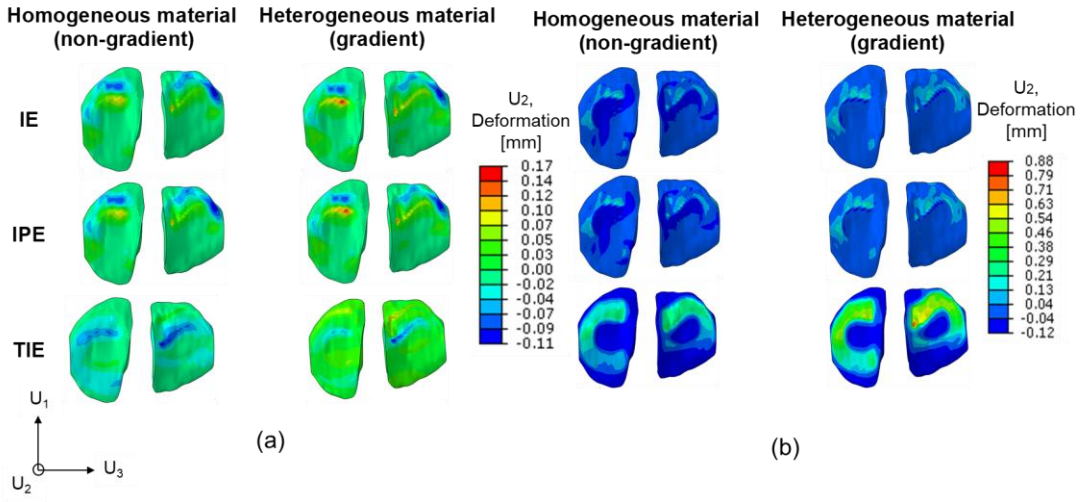

Fig 5. The cartilage deformation (a) U1 (anterior-posterior) on the tibial surface; (b) U2 (proximal-distal) on the tibial surface at full extension position after loading.

Table 3

The estimated over-prediction of mechanical measures in percentage for homogeneous model relative to its heterogeneous alternative.

Comparison of models	Zones	Mises stress (%)	Max. prin. Stress (%)	Max. prin. log. strain (%)	Min. prin. log. strain (%)	Max. def. (%)	Max. pres. generated (%)
Homo. IE	SZ	25	32	9	28	6	0.3
Vs	TZ	12	5	10	13	7	6
Hetro. IE	DZ	4	15	22	28	6	12
Homo. IPE	SZ	25	36	49	42	5	0.7
Vs	TZ	14	6	8	99	4	6
Hetro. IPE	DZ	22	15	23	4	5	12
Homo. TIE	SZ	60	42	4	95	3	47
Vs	TZ	4	88	71	98	3	37
Hetro. TIE	DZ	37	215	42	27	2	47

Note: Homogeneous isotropic elastic (Homo. IE), heterogeneous isotropic elastic (Hetro. IE), homogeneous isotropic poroelastic (Homo. IPE), heterogeneous isotropic poroelastic (Hetro. IPE), homogeneous transversely isotropic elastic (Homo. TIE), heterogeneous transversely isotropic elastic

(Hetro. IE), maximum principal (Max. prin.), maximum principal logarithmic strain (Max. prin. log. strain), maximum deformation (Max. def.), the maximum pressure (Max. pres.)

The tibial cartilage deformation U_2 (anterior-posterior) over the medial and lateral compartment of the tibial cartilage surface are shown for different material models and also for the deformation in U_1 (proximal-distal) given by Figure 5(a) and 5(b). The maximum tibial cartilage deformation for the IPE geometrical heterogeneous model is 0.17 mm in the posterior and 0.88 mm in the proximal direction, where the solid model has lesser deformation. It indicates that porosity impacts tibial deformation and pressure distribution in a knee joint during the standing position. It can be observed from Figure 5 that even with the homogeneous TIE model, the in-plane (anterior-posterior) and through plane (proximal-distal) cartilage deformation is more pronounced and clear than the material heterogeneous IPE model. Therefore TIE models can safely assumed to be reliable in predicting the onset and progression of OA.

In addition, Table.3 compares the maximum variation in Mises stress, principal stress, strain, deformation, and pressure generated on the cartilage with the homogeneous and heterogeneous entity. The maximum percentage change in stresses and strains is observed higher in the TIE model than in the IE and IPE models. The maximum primary stress varies about 200 percentage in TIE models between homogeneous and heterogeneous entity.

4. Discussion

This study examines the influence of heterogeneous material characteristics as a function of tissue depth from superficial to deep zone with multiple constitutive material models. Also, investigate the impact of stresses and strains during the full extension position (standing position) using the finite element knee model. Verifying

simulation findings is a critical step, and we double-checked that our findings for the intact knee model match those found in the literature[54–59]. The IE, IPE, and TIE cartilage material models are compared with homogeneous and heterogeneous entities. The contact pressure distribution is observed not so evident from IE models compared to IPE or TIE models, and the material heterogeneity produces a relatively lower magnitude of pressure distribution.

According to some studies, the material property of articular cartilage varies enormously with distance from the articular surface, especially in the superficial region; hence heterogeneous constitutive models suit well for such studies[60]. Also, many constitutive models are proposed for implementing intact and OA heterogeneous characteristics. The heterogeneous behavior of a finite element cartilage model with an incompressible, poroelastic solid matrix reinforced by an inhomogeneous, distributed fibre filled with an incompressible fluid in the collagen–proteoglycan solid matrix's is well predicted [7]. The split-line patterns are utilized for FRPE inhomogeneous cartilage models to illustrate diverse cartilage influenced by collagen fibres. The average Mises stresses in the homogeneous IE model are 2.7 MPa in the tibial lateral compartment and 2.2 MPa in the femoral lateral component, similar to the range reported in the previous work[61,62]. Also, with a load of 1000 N, the maximum contact pressure generated on cartilage surface varies between 6 and 16 MPa[63]. Particularly in the geometrically heterogeneous model, the maximum principal stresses increased significantly in the cartilage's middle zone[21]. The early OA model showed increased compressive strains in the articulating layer, as well as decreased stresses and fibril strains, especially in the intermediate zone[33,64].

We assumed that IE models predict more accurate findings under short-term loading, similar to the assumptions made in other investigations[10,65]. Moreover, in

compression, the IE material model (elastic) showed the highest primary stresses, whereas the other models indicated tension. It's because the IE material model doesn't include fluid pressure. According to previous research, the load supported by fluid in cartilage can be as high as 5–15 MPa, which can support 80–90% of the BW when walking[15,28,42] However, different parameters undoubtedly likewise influence the material heterogeneity characteristics in cartilage. This might alter minimally if more attributes were included (heterogeneity in fluid flow across cartilage thickness), but it should not change any conclusions about the correlation between the material models. The IE and IPE models are basic models, which do not take into account of material heterogeneity of the cartilage. From the present study, material heterogeneous TIE models show better impression of meniscus reaction on articular cartilage compared to its homogeneous alternative. While IE and IPE geometrically heterogeneous models predict poor impression on cartilage surface. Hence material heterogeneous TIE model can be used as a better alternative model to fiber reinforced model in knee biomechanics study.

In a wide range of biomedical engineering applications, it is becoming increasingly important to develop better constitutive models for modelling soft tissue deformation. Researchers can use these articular cartilage model comparisons to look into tissue-joint mechanism, implant material design, and have a better understanding of microscale response of tissues.

5. Conclusions

In summary, the following conclusions drawn: (1) the maximum cartilage contact pressure induced by the knee joint with the geometrically heterogeneous material model is lower compared to the homogeneous model; (2) the maximum Von-Mises stress may not present a quantitative assessment of cartilage damage; (3)

Poroelastic cartilage model can be helpful to in estimative anterior/posterior deformation whereas material heterogeneous TIE model is suitable in understanding proximal/distal deformation limits. (4) The maximum change in stresses and strains are observed in TIE models than IE and IPE models.

The study has some limitations in terms of model generation, input, and assumptions. The knee kinematics is very complex, and hard to simulate the exact motion; the tibia stresses are a combination of loading (compression), shear, and tensile. In this article, only the knee joint's standing (full extension) position is considered as a simple case of loading. Other soft tissues are left out (patella, patellar tendon, joint capsule, and skin) in the models because the focus of this investigation is to compare three distinct material models of cartilage having the geometry under same applied load.

Acknowledgement

KKP gratefully acknowledges the financial support of the DST-INSPIRE Faculty Award (File No.: DST/INSPIRE/04/2016/000735), Govt. of India, in executing the computational part of this work.

Declaration of conflicting interests:

The author(s) declared no potential conflicts of interest with respect to the research, authorship and/or publication of this article.

Funding: DST-INSPIRE Faculty Award, Govt. of India

Ethical Approval: Not required

References

1. Gill TJ, Van De Velde SK, Wing DW, et al. Tibiofemoral and patellofemoral kinematics after reconstruction of an isolated posterior cruciate ligament injury: In vivo analysis during lunge. *Am J Sports Med* 2009; 37: 2377–2385.

2. Drake RL, Vogel AW, Mitchell AWM. *Gray's Anatomy for Students*. 4th ed. Philadelphia: Elsevier, 2019.

3. Shirazi R, Shirazi-Adl A. Computational biomechanics of articular cartilage of human knee joint: Effect of osteochondral defects. *J Biomech* 2009; 42: 2458–2465.

4. Smith CR, Vignos MF, Lenhart RL, et al. The influence of component alignment and ligament properties on tibiofemoral contact forces in total knee replacement. *J Biomech Eng*; 138. Epub ahead of print 2016. DOI: 10.1115/1.4032464.

5. Naghibi Beidokhti H, Janssen D, Khoshgoftar M, et al. A comparison between dynamic implicit and explicit finite element simulations of the native knee joint. *Med Eng Phys* 2016; 38: 1123–1130.

6. Haris A, Beng Chye Tan V. Stress response envelopes of intact tibiofemoral joint and knee osteoarthritis. *Proc Inst Mech Eng Part H J Eng Med* 2020; 234: 1151–1161.

7. Pierce DM, Ricken T, Holzapfel GA. A hyperelastic biphasic fibre-reinforced model of articular cartilage considering distributed collagen fibre orientations: Continuum basis, computational aspects and applications. *Computer Methods in Biomechanics and Biomedical Engineering* 2013; 16: 1344–1361.

8. Jurvelin JS, Buschmann MD, Hunziker EB. Mechanical anisotropy of the human knee articular cartilage in compression. *Proc Inst Mech Eng Part H J Eng Med* 2003; 217: 215–219.

9. Sophia Fox AJ, Bedi A, Rodeo SA. The basic science of articular cartilage: Structure, composition, and function. *Sports Health* 2009; 1: 461–468.

10. Tanska P, Mononen ME, Korhonen RK. A multi-scale finite element model for investigation of chondrocyte mechanics in normal and medial meniscectomy human knee joint during walking. *J Biomech* 2015; 48: 1397–1406.

11. Meng Q, An S, Damion RA, et al. The effect of collagen fibril orientation on the biphasic mechanics of articular cartilage. *J Mech Behav Biomed Mater* 2017; 65: 439–453.

12. Changoor A, Nelea M, Méthot S, et al. Structural characteristics of the collagen network in human normal, degraded and repair articular cartilages observed in polarized light and scanning electron microscopies. *Osteoarthr Cartil* 2011; 19: 1458–1468.

13. Kazemi M, Dabiri Y, Li LP. Recent advances in computational mechanics of the human knee joint. *Comput Math Methods Med*; 2013. Epub ahead of print 2013. DOI: 10.1155/2013/718423.

14. Kazemi M, Dabiri Y, Li LP. Recent Advances in Computational Mechanics of the Human Knee Joint. *Comput Math Methods Med* 2013; 2013: 1–27.

15. Bursać PM, Obitz TW, Eisenberg SR, et al. Confined and unconfined stress relaxation of cartilage: appropriateness of a transversely isotropic analysis. *J Biomech* 1999; 32: 1125–1130.

16. Shirazi R, Shirazi-Adl A, Hurtig M. Role of cartilage collagen fibrils networks in knee joint biomechanics under compression. *J Biomech* 2008; 41: 3340–3348.

17. Orozco GA, Tanska P, Mononen ME, et al. The effect of constitutive representations and structural constituents of ligaments on knee joint mechanics. *Sci Rep* 2018; 8: 1–15.

18. Julkunen P, Wilson W, Jurvelin JS, et al. Stress-relaxation of human patellar articular cartilage in unconfined compression: Prediction of mechanical response by tissue composition and structure. *J Biomech* 2008; 41: 1978–1986.

19. Halonen KS, Dzialo CM, Mannisi M, et al. Workflow assessing the effect of gait alterations on stresses in the medial tibial cartilage - Combined musculoskeletal modelling and finite element analysis. *Sci Rep* 2017; 7: 1–14.

20. Meng Q, Jin Z, Wilcox R, et al. Computational investigation of the time-dependent contact behaviour of the human tibiofemoral joint under body weight. *Proc Inst Mech Eng Part H J Eng Med* 2014; 228: 1193–1207.

21. Halonen KS, Mononen ME, Jurvelin JS, et al. Importance of patella, quadriceps forces, and depthwise cartilage structure on knee joint motion and cartilage response during gait. *J Biomech Eng* 2016; 138: 1–11.

22. Faisal TR, Adouni M, Dhaher YY. The effect of fibrillar degradation on the mechanics of articular cartilage: a computational model. *Biomech Model Mechanobiol* 2019; 18: 733–751.

23. Venäläinen MS, Mononen ME, Salo J, et al. Quantitative Evaluation of the Mechanical Risks Caused by Focal Cartilage Defects in the Knee. *Sci Rep* 2016; 6: 1–12.

24. Trad Z, Barkaoui A, Chafra M, et al. Finite element analysis of the effect of high tibial osteotomy correction angle on articular cartilage loading. *Proc Inst Mech Eng Part H J Eng Med* 2018; 232: 553–564.

25. Donahue TLH, Hull ML, Rashid MM, et al. A finite element model of the human knee joint for the study of tibio-femoral contact. *J Biomech Eng* 2002; 124: 273–280.

26. Zhang K, Li L, Yang L, et al. Effect of degenerative and radial tears of the meniscus and resultant meniscectomy on the knee joint: a finite element analysis. *J Orthop Transl*

2019; 18: 20–31.

27. Li L, Yang X, Yang L, et al. Biomechanical analysis of the effect of medial meniscus degenerative and traumatic lesions on the knee joint. *Am J Transl Res* 2019; 11: 542–556.

28. Ateshian GA, Wang H, Lai WM. The role of interstitial fluid pressurization and surface porosities on the boundary friction of articular cartilage. *J Tribol* 1998; 120: 241–248.

29. Klets O, Mononen ME, Tanska P, et al. Comparison of different material models of articular cartilage in 3D computational modeling of the knee: Data from the Osteoarthritis Initiative (OAI). *J Biomech* 2016; 49: 3891–3900.

30. Suh JK, Disilvestro MR. Biphasic poroviscoelastic behavior of hydrated biological soft tissue. *J Appl Mech Trans ASME* 1999; 66: 528–535.

31. Orozco GA, Tanska P, Mononen ME, et al. The effect of constitutive representations and structural constituents of ligaments on knee joint mechanics. *Sci Rep* 2018; 8: 1–15.

32. Bolcos PO, Mononen ME, Mohammadi A, et al. Comparison between kinetic and kinetic-kinematic driven knee joint finite element models. *Sci Rep* 2018; 8: 1–11.

33. Klets O, Mononen ME, Liukkonen MK, et al. Estimation of the Effect of Body Weight on the Development of Osteoarthritis Based on Cumulative Stresses in Cartilage: Data from the Osteoarthritis Initiative. *Ann Biomed Eng* 2018; 46: 334–344.

34. Liukkonen MK, Mononen ME, Tanska P, et al. Application of a semi-automatic cartilage segmentation method for biomechanical modeling of the knee joint. *Comput Methods Biomech Biomed Engin* 2017; 20: 1453–1463.

35. Deneweth JM, McLean SG, Arruda EM. Evaluation of hyperelastic models for the non-linear and non-uniform high strain-rate mechanics of tibial cartilage. *J Biomech* 2013; 46: 1604–1610.

36. Jeffery AK, Blunn GW, Archer CW, et al. Three-dimensional collagen architecture in bovine articular cartilage. *J Bone Jt Surg - Ser B* 1991; 73: 795–801.

37. Clark JM. Variation of collagen fiber alignment in a joint surface: A scanning electron microscope study of the tibial plateau in dog, rabbit, and man. *J Orthop Res* 1991; 9: 246–257.

38. Mizrahi J, Maroudas A, Lanir Y, et al. The ‘instantaneous’ deformation of cartilage: Effects of collagen fiber orientation and osmotic stress. *Biorheology* 1986; 23: 311–330.

39. Marchi BC, Arruda EM, Coleman RM. The Effect of Articular Cartilage Focal Defect

418 Size and Location in Whole Knee Biomechanics Models. *J Biomech Eng*; 142. Epub
419 ahead of print 2020. DOI: 10.1115/1.4044032.

420 40. Hosoda N, Sakai N, Sawae Y, et al. Finite Element Analysis of Articular Cartilage
421 Model Considering the Configuration and Biphasic Property of the Tissue. *IFMBE Proc*
422 2009; 23: 1883–1887.

423 41. Marchi BC, Arruda EM. A study on the role of articular cartilage soft tissue constitutive
424 form in models of whole knee biomechanics. *Biomechanics and Modeling in*
425 *Mechanobiology* 2017; 16: 117–138.

426 42. Halonen KS, Mononen ME, Jurvelin JS, et al. Deformation of articular cartilage during
427 static loading of a knee joint - Experimental and finite element analysis. *J Biomech*
428 2014; 47: 2467–2474.

429 43. Tomic A, Grillo A, Federico S. Poroelastic materials reinforced by statistically oriented
430 fibres-numerical implementation and application to articular cartilage. *IMA J Appl Math*
431 *(Institute Math Its Appl* 2014; 79: 1027–1059.

432 44. Raju V, Koorata PK, Kamat Y. Case study for contact pressure improvisation with
433 graded implant material in articular cartilages of knee joint. *J Mech Sci Technol* 2021;
434 35: 1049–1054.

435 45. Erdemir A, Sibole S. Open Knee: A Three-Dimensional Finite Element Representation
436 of the Knee Joint. *User's Guid Version 100*, https://simtk.org/home/openknee (2010).

437 46. Erdemir A. Open Knee: Open Source Modeling and Simulation in Knee Biomechanics. *J*
438 *Knee Surg* 2014; 29: 107–116.

439 47. Smith M. *ABAQUS/Standard User's Manual, Version 6.9*. Providence, United States:
440 Dassault Systèmes Simulia Corp, 2009.

441 48. Wilson W, Van Donkelaar CC, Van Rietbergen B, et al. Stresses in the local collagen
442 network of articular cartilage: A poroviscoelastic fibril-reinforced finite element study. *J*
443 *Biomech* 2004; 37: 357–366.

444 49. Vaziri A, Nayeb-Hashemi H, Singh A, et al. Influence of meniscectomy and meniscus
445 replacement on the stress distribution in human knee joint. *Annals of Biomedical*
446 *Engineering* 2008; 36: 1335–1344.

447 50. Wilson W, Van Rietbergen B, Van Donkelaar CC, et al. Pathways of load-induced
448 cartilage damage causing cartilage degeneration in the knee after meniscectomy. *J*
449 *Biomech* 2003; 36: 845–851.

450 51. Imeni M, Seyfi B, Fatouraee N, et al. Constitutive modeling of menisci tissue: a critical

review of analytical and numerical approaches. *Biomech Model Mechanobiol*. Epub ahead of print 2020. DOI: 10.1007/s10237-020-01352-1.

52. Peña E, Calvo B, Martínez MA, et al. A three-dimensional finite element analysis of the combined behavior of ligaments and menisci in the healthy human knee joint. *J Biomech* 2006; 39: 1686–1701.

53. Łuczkiewicz P, Daszkiewicz K, Witkowski W, et al. Influence of meniscus shape in the cross sectional plane on the knee contact mechanics. *J Biomech* 2015; 48: 1356–1363.

54. Morimoto Y, Ferretti M, Ekdahl M, et al. Tibiofemoral Joint Contact Area and Pressure After Single- and Double-Bundle Anterior Cruciate Ligament Reconstruction. *Arthrosc - J Arthrosc Relat Surg* 2009; 25: 62–69.

55. Marzo JM, Gurske-DePerio J. Effects of medial meniscus posterior horn avulsion and repair on tibiofemoral contact area and peak contact pressure with clinical implications. *Am J Sports Med* 2009; 37: 124–129.

56. Allaire R, Muriuki M, Gilbertson L, et al. Biomechanical consequences of a tear of the posterior root of the medial meniscus: Similar to total meniscectomy. *J Bone Jt Surg - Ser A* 2008; 90: 1922–1931.

57. Lee SJ, Aadalen KJ, Malaviya P, et al. Tibiofemoral contact mechanics after serial medial meniscectomies in the human cadaveric knee. *Am J Sports Med* 2006; 34: 1334–1344.

58. Paletta GA, Manning T, Snell E, et al. The effect of aiiograft meniscal replacement on intraarticular contact area and pressures in the human knee: A biomechanical study. *Am J Sports Med* 1997; 25: 692–698.

59. Halonen KS, Mononen ME, Töyräs J, et al. Optimal graft stiffness and pre-strain restore normal joint motion and cartilage responses in ACL reconstructed knee. *J Biomech* 2016; 49: 2566–2576.

60. Chen AC, Bae WC, Schinagl RM, et al. Depth- and strain-dependent mechanical and electromechanical properties of full-thickness bovine articular cartilage in confined compression. *J Biomech* 2001; 34: 1–12.

61. Yang NH, Canavan PK, Nayeb-Hashemi H. The effect of the frontal plane tibiofemoral angle and varus knee moment on the contact stress and strain at the knee cartilage. *J Appl Biomech* 2010; 26: 432–443.

62. Yang NH, Canavan PK, Nayeb-Hashemi H, et al. Protocol for constructing subject-specific biomechanical models of knee joint. *Comput Methods Biomech Biomed Engin*

2010; 13: 589–603.

63. Mononen ME, Mikkola MT, Julkunen P, et al. Effect of superficial collagen patterns and fibrillation of femoral articular cartilage on knee joint mechanics-A 3D finite element analysis. *J Biomech* 2012; 45: 579–587.

64. Liukkonen MK, Mononen ME, Klets O, et al. Simulation of subject-specific progression of knee osteoarthritis and comparison to experimental follow-up data: Data from the osteoarthritis initiative. *Sci Rep* 2017; 7: 1–14.

65. Mononen ME, Jurvelin JS, Korhonen RK. Implementation of a gait cycle loading into healthy and meniscectomised knee joint models with fibril-reinforced articular cartilage. *Comput Methods Biomech Biomed Engin* 2015; 18: 141–152.